Velocity shear, turbulent saturation, and steep plasma gradients in the scrape-off layer of inner-wall limited tokamaks

IOP Publishing | International Atomic Energy Agency Nuclear Fusion

Nucl. Fusion **57** (2017) 034001 (6pp) doi:10.1088/1741-4326/aa4eb6

Letter

Velocity shear, turbulent saturation, and steep plasma gradients in the scrape-off layer of inner-wall limited tokamaks

F.D. Halpern[1,2] **and P. Ricci**[1]

[1] École Polytechnique Fédérale de Lausanne (EPFL), Swiss Plasma Center, CH-1015 Lausanne, Switzerland
[2] General Atomics, PO Box 85608, San Diego, CA 92186-5608, USA

E-mail: halpernf@fusion.gat.com

Received 3 October 2016, revised 31 October 2016
Accepted for publication 10 November 2016
Published 19 December 2016

Abstract

The narrow power decay-length (λ_q), recently found in the scrape-off layer (SOL) of inner-wall limited (IWL) discharges in tokamaks, is studied using 3D, flux-driven, global two-fluid turbulence simulations. The formation of the steep plasma profiles is found to arise due to radially sheared $\mathbf{E}\times\mathbf{B}$ poloidal flows. A complex interaction between sheared flows and parallel plasma currents outflowing into the sheath regulates the turbulent saturation, determining the transport levels. We quantify the effects of sheared flows, obtaining theoretical estimates in agreement with our non-linear simulations. Analytical calculations suggest that the IWL λ_q is roughly equal to the turbulent correlation length.

Keywords: heat-flux width, plasma turbulence, scrape-off layer, sheared flows

(Some figures may appear in colour only in the online journal)

Sheared flows can significantly affect the properties of turbulence in magnetically confined plasmas. These effects are observed in many plasma configurations, an archetype of such phenomena being the spontaneous formation of the high-confinement (H-)mode barrier at the edge of tokamak plasmas [1]. Turbulent suppression typically occurs when the radial shearing rate of the $\mathbf{E}\times\mathbf{B}$ plasma flows, $\omega_{\mathbf{E}\times\mathbf{B}} = \mathrm{d}v_{\mathbf{E}\times\mathbf{B}}/\mathrm{d}r$ ($v_{\mathbf{E}\times\mathbf{B}} = \mathbf{E}\times\mathbf{B}/B^2$), is of the order of the linear growth rate of the turbulent modes [2, 3]. Understanding the effects of sheared flows is paramount for attaining a fusion reactor, in particular due to their typically beneficial effects upon plasma energy confinement and stability.

The present letter deals with radially sheared $\mathbf{E}\times\mathbf{B}$ flows in the scrape-off layer (SOL) of tokamak plasmas. In this region of the device, the balance between cross-field heat transport against parallel streaming along magnetic field lines gives rise to exponentially decaying power profiles with a characteristic length $\lambda_q = -(d_x \ln q_\parallel)^{-1}$ ($q_\parallel \sim nc_sT$, with $c_s = \sqrt{(T_\mathrm{e}+T_\mathrm{i})/m_\mathrm{i}}$, is the power flowing along the magnetic field lines towards the device walls, and x is the radial coordinate). As opposed to the confined plasma region, where we seek to use sheared flows to minimize turbulent transport, SOL turbulence can be helpful by broadening profiles to avoid a too narrow power exhaust channel.

We concentrate on the inner-wall limited (IWL) geometry, where the plasma makes contact with the inner-wall of the device. This configuration will be used as a start-up plasma scenario in ITER before standard X-point configuration is attained [4]. It was originally assumed that the ITER IWL SOL could be described with a single-exponential λ_q of a few cm's [5]. Recent IWL experiments demonstrated that the SOL plasma profiles have a double-exponential decay length structure. In effect, in the near-SOL just outside the confined plasma region, λ_q is an order of magnitude smaller than expected [6–10]. We refer to this steep gradient region as the 'narrow heat-flux feature'. A multi-device study projects that

the ITER IWL near-SOL λ_q will be about 4 mm, and prompted a redesign of the inner-wall tiles to accommodate for the significantly smaller than expected λ_q [11].

Herein we demonstrate that the steep gradients in the narrow heat-flux feature can arise due to radially sheared $\mathbf{E}\times\mathbf{B}$ poloidal flows present at the interface between the confined plasma region and the SOL. We observe this phenomenon in 3D flux-driven turbulence simulations of plasma dynamics in the IWL configuration. Despite the strongly sheared flows, we find a relative fluctuation amplitude of about 20% within the narrow feature in the simulations, which is consistent with experimental observations. The most peculiar and surprising aspect of the simulated dynamics is the role of sheath currents and their interaction with the sheared turbulent flows in regulating cross-field turbulent transport. Considering these phenomena, we develop a reduced transport model capturing the physical mechanisms at play within the narrow feature. The resulting λ_q is intimately linked to the turbulent correlation length.

The formation of a narrow heat-flux feature is demonstrated using 3D flux-driven turbulence simulations of plasma dynamics in the IWL configuration. The non-linear simulations allow us to extract and understand the variation of the near-SOL λ_q with the plasma parameters. We make use of the drift-reduced Braginskii equations [12], which arise from applying the orderings $\mathrm{d}/\mathrm{d}t \ll \omega_{ci}$ ($\omega_{ci} = eB/m_\mathrm{i}$ is the ion gyrofrequency, with the value of B taken from the magnetic axis) and $k_\perp \gg k_\parallel$ to the Braginskii fluid equations [13]. We consider the simplest possible model that can be used to recover the narrow heat-flux feature, i.e. electrostatic, cold ions, a large aspect ratio torus with circular geometry, and we use the Boussinesq approximation. This model includes the physics of drift and ballooning modes, which can be destabilized either by finite resistivity or electron inertia. The model equations for conservation of density n, vorticity $\Omega = \nabla_\perp^2\phi$, parallel electron and ion velocities $v_{\parallel\mathrm{e,i}}$, and electron temperature T_e read

$$\frac{\mathrm{d}n}{\mathrm{d}t} = \frac{2}{eB}\left[\hat{C}(p_\mathrm{e}) - en\hat{C}(\phi)\right] - \nabla\cdot\left(nv_{\parallel\mathrm{e}}\hat{\mathbf{b}}\right) + D_n\nabla_\perp^2 n + S_n \tag{1}$$

$$\frac{\mathrm{d}\,\Omega}{\mathrm{d}t} = \frac{2B}{nm_\mathrm{i}}\hat{C}(p_\mathrm{e}) + \frac{B^2}{nm_\mathrm{i}}\nabla\cdot\left(j_\parallel\hat{\mathbf{b}}\right) - v_{\parallel\mathrm{i}}\nabla_\parallel\Omega + D_\Omega\nabla_\perp^2\,\Omega + \frac{B}{3nm_\mathrm{i}}\hat{C}(G_\mathrm{i}) \tag{2}$$

$$\frac{\mathrm{d}v_{\parallel\mathrm{e}}}{\mathrm{d}t} = \frac{ej_\parallel}{\sigma_\parallel m_\mathrm{e}} + \frac{e\nabla_\parallel\phi}{m_\mathrm{e}} - \frac{\nabla_\parallel p_\mathrm{e}}{nm_\mathrm{e}} - \frac{0.71\nabla_\parallel T_\mathrm{e}}{m_\mathrm{e}} - v_{\parallel\mathrm{e}}\nabla_\parallel v_{\parallel\mathrm{e}} + D_{v_{\parallel\mathrm{e}}}\nabla_\perp^2 v_{\parallel\mathrm{e}} - \frac{2\nabla_\parallel G_\mathrm{e}}{3nm_\mathrm{e}} \tag{3}$$

$$\frac{\mathrm{d}v_{\parallel\mathrm{i}}}{\mathrm{d}t} = -\frac{\nabla_\parallel p_\mathrm{e}}{n} - v_{\parallel\mathrm{i}}\nabla_\parallel v_{\parallel\mathrm{i}} + D_{v_{\parallel\mathrm{i}}}\nabla_\perp^2 v_{\parallel\mathrm{i}} - \frac{2\nabla_\parallel G_\mathrm{i}}{3nm_\mathrm{i}} \tag{4}$$

$$\frac{\mathrm{d}T_\mathrm{e}}{\mathrm{d}t} = \frac{4}{3}\frac{T_\mathrm{e}}{eB}\left[\frac{7}{2}\hat{C}(T_\mathrm{e}) + \frac{T_\mathrm{e}}{n}\hat{C}(n) - e\hat{C}(\phi)\right] + \frac{2T_\mathrm{e}}{3en}\left[0.71\nabla\cdot\left(j_\parallel\hat{\mathbf{b}}\right) - en\nabla\cdot\left(v_{\parallel\mathrm{e}}\hat{\mathbf{b}}\right)\right] - v_{\parallel\mathrm{e}}\nabla_\parallel T_\mathrm{e} + \chi_{\perp,e}\nabla_\perp^2 T_\mathrm{e} + \chi_{\parallel,e}\nabla_\parallel^2 T_\mathrm{e} + S_{T_\mathrm{e}} \tag{5}$$

In these equations, $\mathrm{d}f/\mathrm{d}t = \partial f/\partial t + \{\phi, f\}/B$, we use the Poisson bracket $\{g, f\} = \hat{\mathbf{b}}\cdot(\nabla g\times\nabla f)$, and the curvature operator $\hat{C}(f) = (B/2)(\nabla\times(\hat{\mathbf{b}}/B))\cdot\nabla f$. The unit magnetic field vector is $\hat{\mathbf{b}} = \mathbf{B}/B$, $j_\parallel = en(v_{\parallel\mathrm{i}} - v_{\parallel\mathrm{e}})$ is the parallel current, and $\sigma_\parallel$ is the Spitzer conductivity. The coordinate system is given by the poloidal length, radial, and toroidal angle coordinates ($y = \theta a, x, \varphi$). S_{T_e} and S_n represent source terms used to inject density and temperature into the simulation domain. The numerical implementation of (1)–(5), including the definition of the gyroviscous terms $\sim G_\mathrm{e,i}$ and other dissipative contributions, is described in detail in [14]. (It has been checked that the artificial dissipation terms do not affect the λ_q simulation results.) Sheath boundary conditions, modeling the interface between the SOL plasma and the vessel walls, are applied at the entrance of the magnetized pre-sheath where the ion drift approximation breaks down [15].

Simulations are carried out within the parameter range $\rho_\star^{-1} = R/\rho_{s0} = 250$–$1000$, $\nu = e^2 n_{\mathrm{e,LCFS}} c_{s0}/(m_\mathrm{i}\sigma_\parallel R) = 0.01, 0.1, 1$, $q = 4$–16, $m_\mathrm{e}/m_\mathrm{i} = 1/200$, with $a/R \approx 1/4$ ($q \approx (r/R)(B_\phi/B_\theta)$ is the magnetic safety factor, while $\rho_{s0} = c_{s0}/\omega_{ci}$, $c_{s0} = \sqrt{T_{\mathrm{e,LCFS}}/m_\mathrm{i}}$). The simulation parameters $\rho_\star^{-1} = 2000$, $\nu = 0.01$ roughly translate to the IWL SOL parameters of Alcator C-Mod ($R_0 = 0.67$ m, $B_0 = 4$ T, $T_{\mathrm{e,LCFS}} = 25$ eV, $n_{\mathrm{e,LCFS}} = 10^{19}$ m^{-3}). Using a simulation with $\rho_\star^{-1} = 500$, $q = 4$, and $\nu = 0.01$, e.g. corresponding to C-Mod parameters but with $B_0 = 1$ T, we illustrate the basic physics mechanisms giving rise to the narrow heat-flux feature. The simulation domain entails an annular volume representing the plasma edge and the SOL, where an infinitely thin wedge acts as a limiter on the high-field-side. Temperature and density are added within the plasma edge using poloidally uniform, radially Gaussian sources (S_{T_e} and S_n) of radial width $5\rho_{s0}$ and placed at the inner boundary of the simulation domain. The plasma profiles steepen due to the action of the sources, driving turbulent modes that fill the SOL with plasma. Figure 1 shows steady-state, poloidally and toroidally averaged, radial profiles of nc_sT_e showing a very clear break in slope about $20\rho_{s0}$ away from the LCFS ($nc_sT_\mathrm{e} \sim q_\parallel$ near the limiter). The near SOL has $\lambda_q \approx 8\rho_{s0}$, which translates to a few millimeters in physical units (typically $\rho_{s0} < 1$ mm), and would be comparable to measured values [11]. Profiles have been obtained just above or below the limiter, and on the outboard midplane in order to demonstrate that the radial gradients are steep on the inboard and outboard planes. From here onwards, we consider time, poloidally and toroidally averaged quantities (denoted with angled brackets $\langle\rangle$) in order to highlight the main physical mechanisms at play. The assumption of weak poloidal

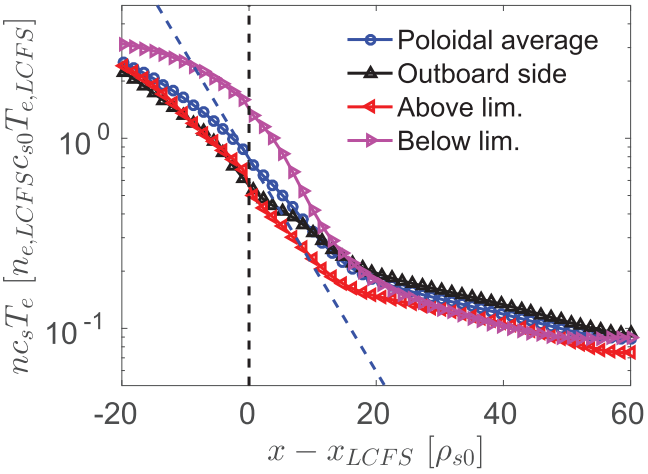

Figure 1. Time averaged radial profiles of nc_sT_e, computed using (*a*) the entire poloidal cross-section (blue dotted line), (*b*) the equatorial outboard side of the device (black line with triangles), and (*c*) just above (red line with left-triangles) and (*d*) below the limiter (magenta line with right-triangles). Data obtained from the quasi steady-state phase of a simulation with $q = 4$, $\rho_\star^{-1} = 500$, $\nu = 0.01$.

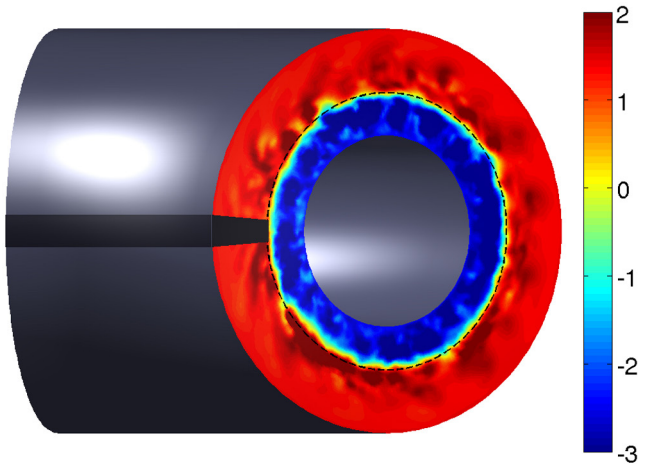

Figure 2. Poloidal cross-section of the electrostatic potential during the quasi steady-state phase of a simulation with $q = 4$, $\rho_\star^{-1} = 500$, $\nu = 0.01$. The wedge on the inner side of the torus represents a toroidal limiter.

gradients is consistent with recent Alcator C-Mod Langmuir probe measurements [16].

Figure 2 shows a snapshot of a poloidal cross-section of ϕ during the quasi-steady state phase of the simulations, where the plasma quantities are subject to power balance. The radial component of the steady-state electric field, $\langle E_x\rangle = -\partial_x\langle\phi\rangle$ has opposite signs in the SOL and in the plasma edge. In the SOL, the interaction between the plasma and the sheath gives $\langle\phi\rangle \sim \Lambda\langle T_e\rangle/e$ ($\Lambda \approx 3$), i.e. $\langle E_x\rangle > 0$, while in the plasma edge $\langle E_x\rangle < 0$. As a result, $\langle\phi\rangle$ varies significantly around the LCFS, giving rise to a poloidal velocity shear layer in our simulations. This shear layer is similar to the one resulting from an imposed electric field well in [17]. In figure 3, the shearing rate $\omega_{\mathbf{E}\times\mathbf{B}} = \rho_\star^{-1}|\langle\phi\rangle''|c_s/R$ is compared against the reference ballooning growth rate [18] $\gamma_b = \sqrt{2\langle T_e\rangle/(\rho_\star L_p)}\,c_s/R$ ($L_p = -d_x\ln\langle p\rangle$). The shear layer effectively divides the edge of the plasma into 3 regions: (a) the plasma edge, where γ_b is comparable or larger than $\omega_{\mathbf{E}\times\mathbf{B}}$, (b) the near-SOL, where drift and ballooning type modes are strongly stabilized due to the velocity shear layer, and (c) the far SOL, where $\omega_{\mathbf{E}\times\mathbf{B}}$ is weak. The latter region was extensively described in our previous studies [19].

We typically find $\Lambda\langle T_e\rangle/e > \langle\phi\rangle$ at the LCFS of our simulations, which is consistent with Langmuir probe measurements in the near-SOL of TCV and COMPASS [8, 9]. This phenomenon, in fact, suggests that parallel currents flowing out of the plasma play an important in the near-SOL, since by charge conservation $j_\perp/L_\perp \sim j_\parallel/L_\parallel$. Assuming that $L_\parallel \approx qR$, this simple heuristic argument immediately relates the near-SOL width, which should be similar to $L_\perp$, to the safety factor $q \sim 1/B_\theta$. Indeed, a simulation scan over $q = 4$–16, shown in figure 4, confirms that $\lambda_q/\rho_s \propto q$ at fixed $\nu = 0.01$ and $\rho_\star^{-1} = 500$. The error bars give the root-mean-square deviation obtained from fitting $\langle nc_sT_e\rangle$ over a time interval of $40R_0/c_{s0}$.

Additional simulation scans have been carried out varying ν and $\rho_\star$ at fixed $q = 4$. In the first case, the resistivity only has an effect when $\nu \sim 1$, in which case we observe weaker $j_\parallel$ near the limiter and an increased radial transport. Within the explored parameter range, we find little variation of λ_q/ρ_s with $\rho_\star$, which suggests a weak dependence on the normalized plasma size.

To gain further insight on the role of the outflowing currents, we concentrate on the charge balance in the system, equation (2). This is illustrated in figure 5, where we have separated the contributions of all the terms in the vorticity equation (including numerical dissipative terms), as radial profiles. We observe that the parallel current contribution, $\left\langle B^2\nabla\cdot j_\parallel/(nm_i)\right\rangle$, strongly affects the charge balance in the near-SOL. The parallel currents are mostly compensated through a polarization contribution $\sim \langle\{\phi,\Omega\}/B\rangle$, while other terms play a minor role. The curvature term $2\left\langle B\hat{C}(p_e)/(nm_i)\right\rangle$ plays an important role in the far-SOL, consistent with blob filament motion [20]. On the other hand, the radial dissipative terms become noticeable near the LCFS due to the steep gradients of the radial $\langle\Omega\rangle$ profile—it has been tested that decreasing the radial diffusion steepens the profile by about $1\rho_{s0}$, which is within the 95% confidence interval of the λ_q fit.

We now propose a reduced model predicting λ_q, based upon a balance between the $j_\parallel$ and $j_\perp$ contributions. Our objective is to obtain the transport levels within the narrow heat-flux feature. The perturbed electrostatic potential is determined through the vorticity balance, allowing us to evaluate the near-SOL $\mathbf{E}\times\mathbf{B}$ velocity. Consider a steady-state equation balancing parallel and polarization current terms at the LCFS. Integrating along the field line, and neglecting parallel mode anisotropy, we obtain

$$\frac{1}{B^2}\{\phi,\Omega\} = \frac{c_s\omega_{ci}}{L_\parallel}\exp\left(\frac{e\delta\phi_{fl}}{T_e}\right), \qquad (6)$$

where we used Gauss' theorem and simplified the sheath current $j_{sh} = enc_s(1-\exp(\Lambda - e\phi/T_e)) \approx enc_s\exp(e\delta\phi_{fl}/T_e)$

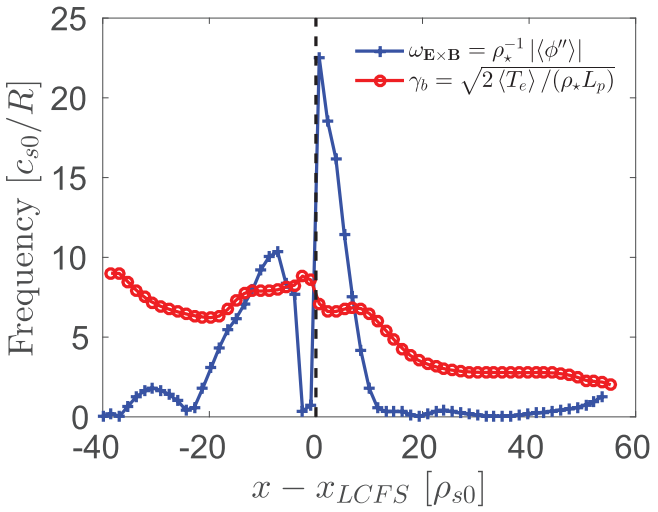

Figure 3. Radial profiles of $\omega_{\mathbf{E}\times\mathbf{B}} = \rho_\star^{-1}|\langle\phi\rangle''|$, and the ballooning growth rate, $\gamma_b = \sqrt{2\langle T_e\rangle/(\rho_\star L_p)}$. Computed from a simulation with $q = 4$, $\rho_\star^{-1} = 500$, $\nu = 0.01$.

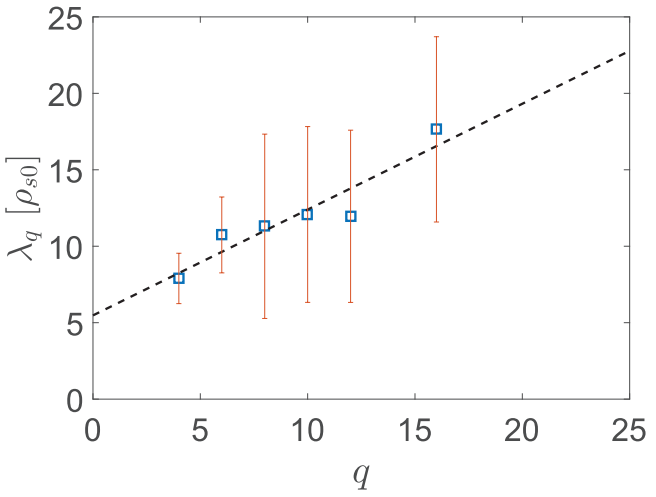

Figure 4. Simulated narrow-feature widths in simulations with $q = 4$–16, $\rho_\star^{-1} = 500$, $\nu = 0.01$.

$(\delta\phi_{fl} = \Lambda T_e/e - \phi)$. The simulation results indicate that the polarization current contribution is dominated by a radially sheared convection of vorticity. Taking a poloidal average, we recover the expression

$$\left\langle \frac{1}{B^2}\frac{\partial}{\partial x}\left(\tilde{\Omega}\,\frac{\partial\tilde{\phi}}{\partial y}\right)\right\rangle \approx \left\langle \frac{c_s\omega_{ci}}{L_\parallel}\exp\left(\frac{e\delta\phi_{fl}}{T_e}\right)\right\rangle, \qquad (7)$$

with the tildes indicating perturbed quantities. This step points out that it is the radial shear of the turbulent motion that allows diverging parallel currents to arise. The currents flowing into the sheath, in turn, allow the potential to decouple from the temperature profile. The interaction with the closed magnetic field line region, where the electric field has the opposite sign than in the SOL, leads thereafter to the radially sheared electric field characteristic of the narrow heat-flux feature.

Next, we estimate $\tilde{\Omega} = -k_\perp^2\tilde{\phi}$, and $\partial_x \sim k_x$ and $\partial_y \sim k_y$, which leads to the radial $\mathbf{E}\times\mathbf{B}$ velocity of turbulent structures propagating across the narrow feature

$$\left\langle \tilde{v}^2_{\mathbf{E}\times\mathbf{B},x}\right\rangle \approx \left\langle \frac{c_s\omega_{ci}}{L_\parallel}\frac{k_y}{k_x k_\perp^2}\exp\left(\frac{e\delta\phi_{fl}}{T_e}\right)\right\rangle. \qquad (8)$$

The turbulent flux follows immediately from the estimate $\langle\Gamma_\perp\rangle \approx \left\langle \tilde{p}\,\tilde{v}_{\mathbf{E}\times\mathbf{B},x}\right\rangle$. The amplitude of the fluctuations traversing the narrow feature from the edge is estimated as $\langle\tilde{p}\rangle \sim \langle p\rangle/(k_x\lambda_q)$ [21, 22]. Then, the near-SOL width can be obtained by balancing $\nabla\cdot\langle\Gamma_\perp\rangle$ against the sheath contribution $\nabla_\parallel\cdot\left\langle\Gamma_\parallel\right\rangle \approx \left\langle pc_s\exp(e\delta\phi_{fl}/T_e)\right\rangle/L_\parallel$. The assumption of parallel convection rather than conduction is justified in the case of weak poloidal plasma gradients, which was an assumption of our analysis. The result is

$$\lambda_q = \left\langle \frac{k_y}{k_x^3 k_\perp^2}\frac{L_\parallel}{\rho_s}\exp\left(\frac{-e\delta\phi_{fl}}{T_e}\right)\right\rangle^{1/4} \approx \frac{k_x^{-1}}{2}\left(\frac{q}{\rho_\star}\right)^{1/4}. \qquad (9)$$

In the last expression, we replaced $L_\parallel = qR$ and we assumed that eddys have comparable radial and poloidal wavenumbers, i.e. $k_x \sim k_y \sim k_\perp$ around the LCFS. The near SOL wavenumber is consistent with simulation results, and with gas-puff imaging of SOL turbulence [23]. As the modes traverse into the far SOL, k_x decreases while k_y remains about constant. We also approximate $\exp(-e\delta\phi_{fl}/T_e)^{1/4} \approx 1/2$, based on the LCFS values consistently found throughout our simulation scan. The weak dependence obtained with respect to the plasma parameters can explain, in part, why it is difficult to vary the narrow feature width in experiments—the plasma parameters appear only indirectly, and through the radial correlation length $L_{\rm rad} = \pi/k_x$. Equation (9) is the principal result of the model, and the simpler expression involving k_x^{-1} is evaluated using the radial eddy correlation length from the simulations and compared against λ_q in figure 6. The simulation parameter range is as mentioned above: $q = 4$–16, $\rho_\star^{-1} = 250, 500, 1000$, $\nu = 0.01, 0.1, 1$, with λ_q generally increasing with the safety factor, at $\nu = 1$, and showing a slow variation with respect to the normalized plasma size.

In conclusion, we propose that a narrow layer of radially-sheared poloidal flows, occurring within the near-SOL, is responsible for the steep plasma gradients recently measured in the IWL tokamak experiments. Non-linear, flux-driven turbulent simulations demonstrate the spontaneous formation of $\mathbf{E}\times\mathbf{B}$ shearing rates significantly surpassing the expected linear growth rate of the turbulent modes. Simulation results suggest that λ_q/ρ_s increases with $q \sim I_p^{-1}$, with weaker variation of λ_q with respect to ν or $\rho_\star$. The analysis of the simulations leads us to conclude that the near-SOL turbulent saturation level can be determined by balancing the polarization currents driven by the turbulence against parallel currents that ultimately flow into the limiter. Analytical estimates lead to a gradient length of the order of the turbulent correlation length. The proposed transport model would suggest that a $\lambda_q \sim q \sim I_p^{-1}$ scaling (e.g. as in the drift heuristic model [24]) can originate from

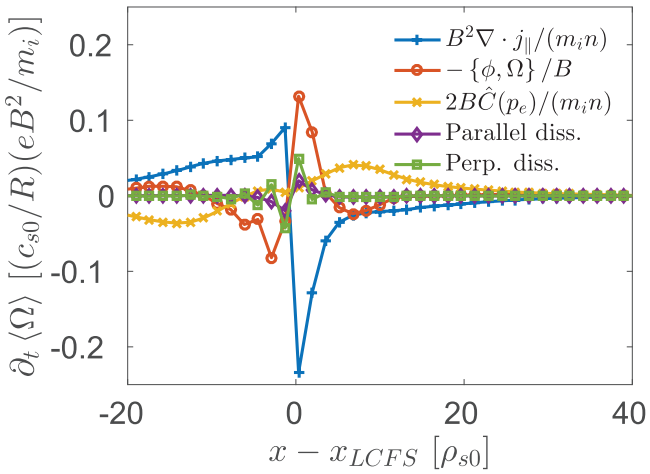

Figure 5. Charge balance contributions from parallel currents (blue line with dots), vorticity convection (red line with crosses), curvature effects (yellow line with x's), parallel (purple line with diamonds) and perpendicular (green line with squares) dissipation terms. Computed from quasi steady-state phase of a simulation with $q = 4$, $\rho_\star^{-1} = 500$, $\nu = 0.01$.

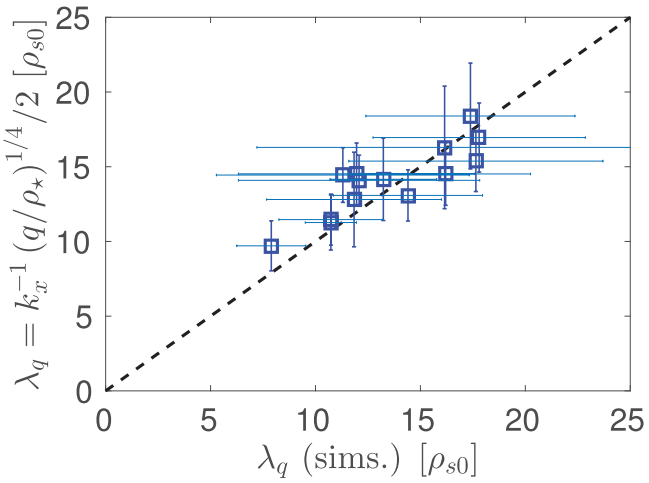

Figure 6. Equation (9) is compared against λ_q from non-linear simulations within the parameter range $q = 4$–16, $\rho_\star^{-1} = 250, 500, 1000$, $\nu = 0.01, 0.1, 1$. The radial correlation length required to evaluate equation (9) was obtained from the simulations.

the turbulent wavenumber. Inertial ballooning modes (IBM) are the most linearly unstable modes in the parameter regime $q = 4$, $\rho_\star^{-1} = 500$, $\nu \approx 0.01$ and with steep plasma gradients [25]. For instance, the wavenumber $k_{\mathrm{IBM}}\rho_s \propto q^{-1}\gamma_b^{-1}$ together with equation (9) yield $\lambda_{q,\mathrm{IBM}}/\rho_s \sim q^{5/6}\rho_\star^{-1/2}\nu^0$.

Note that the elevated shear rate (e.g. satisfying the Waltz quench rule [3]) does not mean that the fluctuations are suppressed within the narrow feature. On the contrary, our simulations indicate elevated relative and absolute RMS fluctuation levels therein. Instead, we argue that the transport dynamics are substantially modified with respect to the local wave-breaking or gradient removal transport paradigm [21, 22]. Our model for the narrow feature can be summarized as follows. The near-SOL fills up with turbulent structures crossing the separatrix. Reynold's stress associated with these structures allows diverging (sheath) parallel currents to arise. Then, the diverging currents force ϕ and T_e to decouple, giving rise to poloidally symmetric sheared flows. The plasma edge dynamics influences the shear rate, although their details do not seem to be crucial to obtain the narrow feature transport levels. As the local linear modes are stabilized by the flow shear ($\gamma < \omega_{\mathbf{E}\times\mathbf{B}}$), the transport level is determined by the convection of turbulent structures, originating within the confined region, across the narrow feature. Their radial velocity, given by equation (8), can be determined using an estimate of the diverging sheath currents. This hypothesis leads to equation (9), which reproduces our simulation results, as shown in figure 6.

As a final remark, we highlight that our results lead to several testable predictions: (a) the turbulent intensity allows the outflow of parallel currents at the limiter, (b) the strength of the currents can be related to k_x, and (c) λ_q can increase with $q \sim 1/B_\theta$. Some of these features, such as the currents at the contact points, have been observed before in several devices. Dedicated experimental campaigns at C-Mod, DIII-D, and TCV will be used with the objective of validating the physical insights here presented.

Acknowledgments

This material is based upon work supported by the U.S. Department of Energy, Office of Science, Office of Fusion Energy Sciences, Theory Program, under Award No. DE-FG02-95ER54309. Part of the simulations presented herein were carried out using the HELIOS supercomputer system at the Computational Simulation Centre of International Fusion Energy Research Centre (IFERC-CSC), Aomori, Japan, under the Broader Approach collaboration between Euratom and Japan, implemented by Fusion for Energy and JAEA. This work has been carried out within the framework of the EUROfusion Consortium and has received funding from the Euratom research and training programme 2014–2018 under grant agreement No 633053, and from the Swiss National Science Foundation. The views and opinions expressed herein do not necessarily reflect those of the European Commission.

References

[1] Wagner F. *et al* 1982 Regime of improved confinement and high beta in neutral-beam-heated divertor discharges of the ASDEX tokamak *Phys. Rev. Lett.* **49** 1408–12

[2] Biglari H., Diamond P.H. and Terry P.W. 1990 Influence of sheared poloidal rotation on edge turbulence *Phys. Fluids* B **2** 1–4

[3] Burrell K.H. 1997 Effects of $E \times B$ velocity shear and magnetic shear on turbulence and transport in magnetic confinement devices *Phys. Plasmas* **4** 1499–518

[4] Pitts R.A., Carpentier S., Escourbiac F., Hirai T., Komarov V., Kukushkin A.S., Lisgo S., Loarte A., Merola M., Mitteau R., Raffray A.R., Shimada M. and Stangeby P.C. 2011 Physics basis and design of the ITER plasma-facing components *J. Nucl. Mater.* **415** S957–64 (*Proc. of the 19th*

Int. Conf. on Plasma-Surface Interactions in Controlled Fusion)
[5] Loarte A. *et al*, The ITPA Scrape-off Layer and Divertor Physics Topical Group 2007 Chapter 4: Power and particle control *Nucl. Fusion* **47** S203
[6] Arnoux G. *et al* and JET-EFDA Contributors 2013 Scrape-off layer properties of ITER-like limiter start-up plasmas in JET *Nucl. Fusion* **53** 073016
[7] Horacek J. *et al* 2014 Narrow heat flux channels in the COMPASS limiter scrape-off layer *J. Nucl. Mater.* **463** 385
[8] Nespoli F., Labit B., Furno I., Canal G.P. and Fasoli A. 2014 Heat loads in inboard limited l-mode plasmas in TCV *J. Nucl. Mater.* **463** 393
[9] Dejarnac R., Stangeby P.C., Goldston R.J., Gauthier E., Horacek J., Hron M., Kocan M., Komm M., Panek R., Pitts R.A. and Vondracek P. 2015 Understanding narrow SOL power flux component in COMPASS limiter plasmas by use of Langmuir probes *J. Nucl. Mater.* **463** 381–4 (*Proc. of the 21st Int. Conf. on Plasma-Surface Interactions in Controlled Fusion Devices (Kanazawa, Japan, 26–30 May 2014)*)
[10] Stangeby P.C., Tsui C.K., Lasnier C.J., Boedo J.A., Elder J.D., Kocan M., Leonard A.W., McLean A.G., Pitts R.A. and Rudakov D.L. 2015 Power deposition on the DIII-D inner wall limiter *J. Nucl. Mater.* **463** 389–92 (*Proc. of the 21st Int. Conf. on Plasma-Surface Interactions in Controlled Fusion Devices (Kanazawa, Japan, 26–30 May 2014)*)
[11] Kocan M. *et al* 2015 Impact of a narrow limiter SOL heat flux channel on the ITER first wall panel shaping *Nucl. Fusion* **55** 033019
[12] Zeiler A., Drake J.F. and Rogers B. 1997 Nonlinear reduced Braginskii equations with ion thermal dynamics in toroidal plasma *Phys. Plasmas* **4** 2134–8
[13] Braginskii S.I. 1965 *Transport Processes in a Plasma* (*Reviews of Plasma Physics* vol 1) (New York: Consultants Bureau)
[14] Halpern F.D., Ricci P., Jolliet S., Loizu J., Morales J., Mosetto A., Musil F., Riva F., Tran T.M. and Wersal C. 2016 The GBS code for tokamak scrape-off layer simulations *J. Comput. Phys.* **315** 388–408
[15] Loizu J., Ricci P., Halpern F.D. and Jolliet S. 2012 Boundary conditions for plasma fluid models at the magnetic presheath entrance *Phys. Plasmas* **19** 122307
[16] Marmar E.S. *et al* 2015 Alcator C-Mod: research in support of ITER and steps beyond *Nucl. Fusion* **55** 104020
[17] Myra J.R., Russell D.A. and D'Ippolito D.A. 2012 Diffusive–convective transition for scrape-off layer transport and the heat-flux width *Plasma Phys. Control. Fusion* **54** 055008
[18] Connor J.W., Hastie R.J. and Taylor J.B. 1978 Shear, periodicity, and plasma ballooning modes *Phys. Rev. Lett.* **40** 396–9
[19] Halpern F.D., Ricci P., Jolliet S., Loizu J. and Mosetto A. 2014 Theory of the scrape-off layer width in inner-wall limited tokamak plasmas *Nucl. Fusion* **54** 043003
[20] Krasheninnikov S.I., D'Ippolito D.A. and Myra J.R. 2008 Recent theoretical progress in understanding coherent structures in edge and SOL turbulence *J. Plasma Phys.* **74** 679–717
[21] Horton W. 1999 Drift waves and transport *Rev. Mod. Phys.* **71** 735–78
[22] Ricci P. and Rogers B.N. 2013 Plasma turbulence in the scrape-off layer of tokamak devices *Phys. Plasmas* **20** 010702
[23] Zweben S.J., Boedo J.A., Grulke O., Hidalgo C., LaBombard B., Maqueda R.J., Scarin P. and Terry J.L. 2007 Edge turbulence measurements in toroidal fusion devices *Plasma Phys. Control. Fusion* **49** S1
[24] Goldston R.J. 2012 Heuristic drift-based model of the power scrape-off width in low-gas-puff H-mode tokamaks *Nucl. Fusion* **52** 013009
[25] Mosetto A., Halpern F.D., Jolliet S. and Ricci P. 2012 Low-frequency linear-mode regimes in the tokamak scrape-off layer *Phys. Plasmas* **19** 112103